THE AMERICAN SOCIETY OF MECHANICAL ENGINEERS
345 E. 47th St., New York, N.Y. 10017

94-GT-37

TURBULENCE MEASUREMENTS IN A HEATED, CONCAVE BOUNDARY LAYER UNDER HIGH FREE-STREAM TURBULENCE CONDITIONS

Michael D. Kestoras
University of Nantes
Nantes, France

Terrence W. Simon
Department of Mechanical Engineering
University of Minnesota
Minneapolis, Minnesota

Abstract

Turbulence measurements for both momentum and heat transfer are taken in a low-velocity, turbulent boundary layer growing naturally over a concave wall. The experiments are conducted with negligible streamwise acceleration and a nominal free-stream turbulence intensity of ~8%. Comparisons are made with data taken in an earlier study in the same test facility but with a 0.6% free-stream turbulence intensity. Results show that elevated free-stream turbulence intensity enhances turbulence transport quantities like $\overline{uv}$ and $\overline{vt}$ in most of the boundary layer. In contrast to the low-turbulence cases, high levels of transport of momentum are measured outside the boundary layer. Stable, Görtler-like vortices, present in the flow under low-turbulence conditions, do not form when the free-stream turbulence intensity is elevated. Turbulent Prandtl numbers, Pr_t, within the log region of the boundary layer over the concave wall increase with streamwise distance to values as high as 1.2. Profiles of Pr_t suggest that the increase in momentum transport with increased free-stream turbulence intensity precedes the increase in heat transport. Distributions of near-wall mixing length for momentum remain unchanged on the concave wall when free-stream turbulence intensity is elevated. Both for this level of free-stream turbulence and for the lower level, mixing length distributions increase linearly with distance from the wall following the standard slope. However when free-stream turbulence intensity is elevated, this linear region extends farther into the boundary layer, indicating the emerging importance of larger eddies in the wake of the boundary layer with the high-turbulence free-stream. Because these eddies are damped by the wall, the influence of the wall grows with eddy size.

Nomenclature

C_f Skin friction coefficient.
C_p Specific heat capacity at constant pressure.
C_{pc} Static pressure coefficient.
G Görtler number, $\frac{U_{pw}\delta_2}{\nu}\sqrt{\frac{\delta_2}{|R|}}$
G_t Turbulent Görtler number, $\frac{U_{pw}\delta_2}{\varepsilon_m}\sqrt{\frac{\delta_2}{|R|}}$
ℓ_m Mixing length of momentum.
L^u_- Free-stream length scale, $\frac{-\left(\overline{u^2}\right)^{3/2}_-}{U_- \frac{d\left(\overline{u^2_-}\right)}{dx}}$
L_ε Dissipation length scale, $\frac{\left(-\overline{uv}\right)^{3/2}}{\varepsilon}$
$P_{-\overline{uv}}$ Production of the shear stress, in the budget equation.
Pr_t Turbulent Prandtl number.
R Radius of curvature (negative for a concave surface).
St Stanton number $q_w/(T_w - T_-)\rho C_p U_{pw}$.
T_- Free-stream mean temperature.
T_w Wall temperature.
$\sqrt{\overline{t^2}}$ Root-mean-square of temperature fluctuations.
$\sqrt{\overline{u^2}}$ Root-mean-square fluctuation of streamwise velocity.
$\overline{u^2}$ Mean square fluctuation of streamwise velocity.
TI Free-stream turbulence intensity.
u Fluctuating component of the streamwise velocity.
U Streamwise mean velocity,
U_{cw} Core velocity extrapolated to wall (same as U_{pw} for low TI cases).
U_- Free-stream streamwise mean velocity.
$\overline{ut}$ Streamwise turbulent heat flux.
$\overline{uv}$ Turbulent shear stress.
$\overline{uv^2}$ Cross-stream transport of turbulent shear stress.
v Fluctuating component of cross-stream velocity.
$\overline{v^2}$ Mean square fluctuation of cross-stream velocity.
$\sqrt{\overline{v^2}}$ Root-mean-square fluctuation of cross-stream velocity.
$\overline{vt}$ Cross-stream turbulent heat flux.
$\overline{v^2t}$ Cross-stream transport of turbulent heat flux.
y Normal distance from the test surface.
$\overline{w^2}$ Mean-square fluctuation of spanwise velocity.

Greek Symbols

δ Momentum boundary layer thickness.

Presented at the International Gas Turbine and Aeroengine Congress and Exposition
The Hague, Netherlands — June 13–16, 1994
This paper has been accepted for publication in the Transactions of the ASME
Discussion of it will be accepted at ASME Headquarters until September 30, 1994

δ_1 Displacement thickness of the boundary layer.

δ_2 Momentum thickness of the boundary layer.

δ_0 Boundary layer thickness at the start of curvature.

$\Delta_{99.5}$ Thermal boundary layer thickness based on 99.5% of the free-stream temperature.

$\delta_{99.5}$ Boundary layer thickness based on 99.5% of the local velocity, obtained by extrapolation of the core velocity distribution toward the wall.

ε Dissipation rate.

ε_h Eddy diffusivity of heat.

ε_m Eddy diffusivity of momentum.

κ Kármán constant.

ν Molecular kinematic viscosity.

Introduction

A review of the literature on the effects of curvature is given in Kestoras and Simon (1992). Concave curvature destabilizes a laminar boundary layer resulting in streamwise vortices, as described by Görtler (1940). These vortices appear when the Görtler number, defined as:

$$G = \frac{U_{pw}\delta_2}{\nu}\sqrt{\frac{\delta_2}{|R|}} \qquad (1)$$

reaches 6 - 10. The formation of vortices in a turbulent boundary layer seems to correlate better with a "turbulent Görtler number," G_t, obtained by replacing the kinematic viscosity with the eddy viscosity, ε_m (Tani, 1962). Shizawa and Honami (1985) suggested that in a turbulent boundary layer, eddy viscosity is large enough that G_t is generally in the stable regime. The present study supports this suggestion. Görtler vortices were obtained in the low-TI comparison case (Kestoras and Simon, 1992). They were established in the pre-transitional, laminar boundary layer for which super-critical Görtler numbers were evaluated and persisted with decreasing effectiveness into the post-transitional flow.

Concave curvature enhances momentum and heat transfer in a turbulent boundary layer. So and Mellor (1975) reported Reynolds normal and shear stresses, and turbulence kinetic energy values that were above flat-wall values. Similar conclusions were reported by Shizawa and Honami (1985). Ramaprian and Shivaprasad (1977) confirmed these findings, remarking that curvature affected $\sqrt{\overline{v^2}}$ more than $\sqrt{\overline{u^2}}$. In a later study, Ramaprian and Shivaprasad (1978) reported that (1) 75% of the $-\overline{uv}$ activity originated from eddies of size greater than $\delta/4$, that (2) mixing lengths, ℓ_m, increased over the concave wall, and that (3) the region of linear growth of ℓ_m extended further into the curved boundary layer than into a straight-wall boundary layer. Hoffmann et al. (1985) confirmed the Ramaprian and Shivaprasad findings and noted that, while convex curvature simply attenuated the turbulent eddies, concave curvature effected a structural change in the boundary layer. Barlow and Johnston (1988) noted that concave curvature amplifies large-scale motions, the single most important source of the increase in Reynolds normal and shear stresses. Further, the structural changes are in two phases; in the first phase, which is complete after a few boundary layer thicknesses[1] downstream of the start of curvature, high-momentum eddies move closer to the wall while low-momentum eddies are driven away from the wall, whereas in the second phase, the large-scale eddies grow and amplify, a process that is completed after about 20 boundary layer thicknesses. Kim et al. (1992) measured turbulent heat fluxes, reporting that in a low-Reynolds number flow, $\overline{vt}$ values at the upwash sites of the Görtler vortices are higher than values at the downwash sites and that turbulent Prandtl numbers are close to unity.

Turbulence intensity, TI, effects are dependent not only on the TI level but also on the free-stream length scale and momentum thickness Reynolds number (Hancock and Bradshaw, 1983, and Blair, 1983). Blair noted that skin friction coefficients and Stanton numbers increase with TI and that, over a flat wall, the logarithmic regions of the velocity and temperature profiles remain unaffected by elevated TI. Over a concave wall, a logarithmic region also remains to $y^+ \approx 100$, unaffected by increased TI (Kestoras and Simon, 1993). Hancock and Bradshaw (1983) reported that free-stream turbulence intensity substantially changes the structure of the outer region of the boundary layer. In the inner region, local equilibrium prevails and the law of the wall remains valid. They also observed that the parameter $\dfrac{\left(\sqrt{\overline{u^2}}/U\right)_{-} \times 100}{L^u_{-}/\delta_{99.5} + 2.0}$ correlated mean-flow data as well as some changes in turbulence structure. Hancock and Bradshaw (1989) experimentally documented the effects of high free-stream turbulence on a turbulent boundary layer over a heated, flat plate. They performed conditionally-sampled measurements on mean and turbulence quantities to separate free-stream (cold) fluid contributions from boundary layer (hot) fluid contributions and reported that the extent of the intermittent region increased with turbulence intensity. The dissipation length, $L_\varepsilon = \dfrac{(-\overline{uv})^{3/2}}{\varepsilon}$ (ε is the dissipation), is little affected by turbulence while the corresponding parameter based on turbulent energy, $\overline{u^2}+\overline{v^2}+\overline{w^2}$, is strongly affected. Thomas and Hancock (1977) experimentally confirming the work of Hunt and Graham (1978) noted that free-stream turbulence is itself affected by the presence of the wall. This effect penetrates one free-stream length scale, L^u_{-}, from the wall. Present measurements support this.

The effect of TI on turbulent boundary layers over curved surfaces has little documentation. Brown and Burton (1977) reported that Stanton numbers were little affected by TI (1.6 % - 9.2 %) over convexly curved surfaces. You et al. (1986) reported that (1) increased levels of TI (0.65 % to 1.85 %) in turbulent boundary layers over a convex wall resulted in reduction of skin friction coefficients and Stanton numbers, that (2) profiles of shear stress reached a state where they ceased to evolve in shape in the streamwise direction, and that (3) curvature effects dominated TI effects.

Data on the effects of free-stream turbulence on turbulent boundary layers over a concave wall are few. Nakano et al. (1981) studied the effects of stable free-stream flow (positive shear) and unstable free-stream flow (negative shear) on a turbulent boundary layer over a concave wall. Under unstable free-stream flow conditions, shear-stress values increased relative to values under stable free-stream flow conditions. Peaks in $\overline{v^2}$ and $\overline{uv}$ profiles were reported at $y/\delta = 0.4$, independent of the free-stream conditions. Kim et al. (1992) reported mean and turbulence measurements over a concave wall. In a high-turbulence case (8%), they reported cross transport of momentum, even in the core flow.

The data in the present study document the growth of a turbulent boundary layer over a concave wall under high-TI conditions. They are taken in the same test facility that Kim et al. (1992) used for their experiments. In a low-TI comparison case to the present case, the authors (Kestoras and Simon, 1992) documented stationary Görtler-like vortices. Skin friction coefficients taken at the downwash and upwash regions of the vortices increased relative to flat-wall values. Stanton numbers remained at the flat-wall values over most of the upstream part of the concave wall, rising noticeably further downstream. Concave curvature increased $\sqrt{\overline{u^2}}$, $\sqrt{\overline{v^2}}$, and $\overline{uv}$ values (Kestoras, 1993). Turbulent heat fluxes, $\overline{vt}$, remained relatively unaffected by the presence of concave curvature, however. Mixing lengths also remained unaffected in the near-wall region, but this region extended farther into the boundary layer. Turbulent Prandtl numbers over the concave wall remained around unity.

In the following paper, turbulence measurements for the same case as that discussed by Kestoras and Simon (1993), are presented

[1] thickness of the boundary layer at the bend entrance

and discussed. Comparison is made to a low-turbulence case which is otherwise the same (Kestoras and Simon, 1992, and Kestoras, 1993). This work expands documentation of the effects of curvature and free-stream turbulence on boundary layers. Enhanced understanding of these effects aids making design decisions for systems where such effects are present, such as highly-loaded turbine airfoils, and provides further support for turbulence closure model development. Results are presented for 8% free-stream turbulence intensity. Though this value is lower than the 10-20% values reported for high-pressure turbine stages, it is sufficiently high to illustrate the free-stream turbulence effect in a flow for which the turbulence can be characterized and replicated. As turbulence levels rise above 10%, the turbulence tends to become anisotropic and facility-specific. Also, for turbulence levels above 10%, there are questions about what can be considered turbulence, versus general unsteadiness.

Test facility and instrumentation.

The facility used to conduct the experiments is an open-circuit, blown-type wind tunnel (Fig. 1). Details of the flow delivery section are given by Wang (1984). Measurements are taken at a nominal velocity of 17.2 m/s. This velocity is uniform to within 0.3 % across the face of the nozzle. The free-stream temperature of the flow is uniform to within 0.1°C.

A free-stream turbulence intensity of ~8 % at the inlet of the test channel is achieved using an insert section downstream of the contraction nozzle. This insert (Kim et al., 1992), consists of a bi-plane grid of 4.2 cm OD PVC pipes on 10.8 cm centers. Downstream of the grid there is a 96.5 cm long development region. The grid is similar to that used by O'Brien and vanFossen (1985) although the blowing feature is not utilized in this study. Free-stream turbulence intensity decays to 4.5 % by the end of the test section. A power spectral distribution (PSD) taken at the nozzle exit shows that 19.6 % of the turbulent energy in the free-stream is uniformly distributed over frequencies below 25 Hz. The level of Tl in the wind tunnel without the turbulence grid is about 0.6 %. The integral length scale of turbulence, measured at the beginning of the test section, is 3.3 cm.

The test channel is rectangular, 68 cm wide, 11 cm deep, and 138 cm long. The test wall is designed to provide a smooth, uniformly-heated surface. It consists of a layer of fiberglass insulation (100 mm), a sheet of Lexan (4.68 mm), an electrical resistance heater (1.56 mm), a thin spacer (25 μm), a Lexan sheet (0.8 mm), and, adjacent to the flow, a layer of liquid crystal (21 μm). Thermocouples embedded within the spacer are distributed both in the streamwise and spanwise directions.

The concave wall has a radius of curvature of 0.97 m and is 1.38 m long. The flexible, outer wall is adjusted to obtain negligible streamwise acceleration: static pressure coefficients, Cp_C, are kept to within 0.03 for the entire test length by movement of the outer wall. Such Cp_C values are based upon static pressures taken at a radial distance of 2 cm from the concave wall. Static pressures were measured using an array of static pressure taps on an end wall. The taps were distributed both in both the streamwise and cross-stream directions.

Data acquisition and processing is performed by a Hewlett Packard series 200, model 16 personal computer. Reynolds stresses are measured using cross wires (TSI 1243 boundary layer "X" probe) of which the prongs are bent at 90° to the probe holder to minimize flow interference. A constant-temperature, four-channel bridge (TSI-IFA-100) is used to power the wires. Simultaneous digitization of the hot wire signals is performed using two Norland (now Hi-Techniques) Prowler digital storage oscilloscopes. For statistical quantities, the sampling rate is 100 Hz, though each sample is acquired in only a few microseconds. Sampling time is at least 40 seconds. Calibrations of the cross wires are in the wind tunnel core flow over a flat section downstream of the concave wall (shown in Fig. 1). They were performed against a total pressure tube after first aligning both the cross-wire probe and the tube with the flow. When the cross-wire probe is aligned, the product of the voltages of the two wires reaches a maximum (Kim, 1986). The Champagne et al. (1967) correction for tangential cooling is applied to Reynolds stress

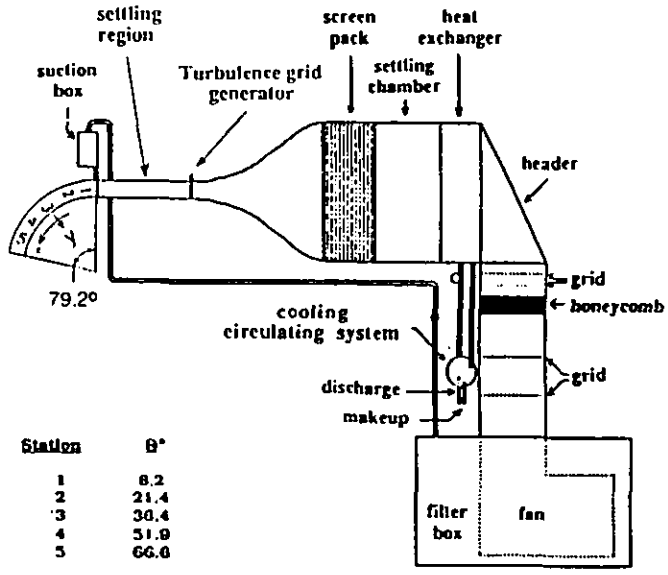

Fig. 1 Schematic Diagram of the Test Facility.

measurements. The uncertainty in $-\overline{uv}$ is 10% of the peak value in the profile. This value is consistent with our experiences in replicating profiles for base cases which are documented in the literature. It is consistent with the careful characterization of uncertainty of hot-wire measurements given by Yavuzkurt (1984).

Turbulent heat fluxes are measured using a specially-designed triple-wire probe (Kim and Simon, 1988). The probe supports two constant-temperature, 2.5 μm diameter wires in an X-configuration for measuring the U- and V- components of the flow. The third wire, 1.3 μm in diameter, is held parallel to one of the two cross-wires. This third wire is operated in the constant-current mode as a resistance temperature detector. Compensation is performed digitally, following the procedure outlined by Hishida and Nagano (1978). A low-noise circuit was built to amplify the cold-wire signal. It was built to also drive the wire with a step function where the current supplied to the cold wire is switched from a high value (up to 6.7 mA) to 1 mA (operating value) to determine the time constant required for digital processing. The hot wires of the heat flux probe are calibrated using the cross-wire probe calibration techniques discussed above. The temperature-resistance calibration of the cold wire is a two-point calibration, using a 0.1°C resolution, mercury-in-glass thermometer. Two Norland Prowler digital oscilloscopes are operated in the master-slave configuration to simultaneously digitize the four traces required: two hot-wire signals, the cold-wire signal and the cold-wire signal time-derivative. The uncertainty in turbulent heat flux measurements is 15 % of the peak value of the profile. This value is determined by comparisons of wall heat flux values with extrapolations of the measurements to the wall for many cases where a constant heat flux zone is expected. Such experience has been gathered over the last five years.

Heat transfer experiments are conducted with the test walls uniformly heated to nominally 193 W/m^2, within 1 % non uniformity (Wang, 1984). Wall temperatures are measured with 76 μm diameter embedded chromel-alumel thermocouples. The thermocouples were calibrated against a platinum-resistance standard. The spacing of the thermocouples in the streamwise direction is 2.54 cm over the concave wall. Wall temperature values for locations between the thermocouple positions are needed to non-dimensionalize temperature profiles. They were obtained by interpolation of the measured values: cubic polynomials were used for this calculation. Surface temperatures are obtained by correcting the thermocouple readings for temperature drops between the locations of the embedded thermocouple beads and the test wall surface. Such corrections were typically 1.2°C of the 5°C thermocouple to free-stream temperature difference. The uncertainty in the wall temperature-readings, thus obtained, is 0.2°C. Careful

measurements of wall material conductivity, contact resistance values and surface emissivity were needed to achieve this uncertainty.

Profiles were taken using a stepping motor assembly. The motor is capable of 400 half-steps per revolution, each half-step equivalent to 5 μm of travel in the y-direction.

Results

Under high free-stream turbulence conditions (TI ~ 8%) the flow appears to be fully turbulent from Station 2 (the first measurement station presented). It was reported in an earlier study that stationary Görtler-like vortices do not form in the high-turbulence case (Kestoras and Simon, 1993). This study, which presents mean velocity and temperature profiles, would serve as useful companion reading to this paper.

In the outer region of the boundary layer, the effects of TI are most profound. In the inner region, the high TI effects are important but the concave curvature is more influential. Based on the data to be presented, the following structural changes of the boundary layer, brought about by high free-stream turbulence, are suggested: High free-stream turbulence provides large-scale, high-streamwise-momentum eddies outside the boundary layer. These eddies are accelerated toward the concave surface inducing an increase in eddy scales within the boundary layer.

The effects of concave curvature are enhanced by cross transport of momentum by boundary work. An explanation of this is given by Eckert (1987) who states that such cross transport takes place when (1) the flow pathlines are curved and (2) the flow is unsteady. Curved pathlines lead to higher pressures on the concave walls of pathtubes than on the convex walls. Unsteadiness results in this pressure difference effecting work by a pathtube on its neighbor on the concave side. One could also look at this process as a "turbulent diffusion" where curvature leads to the establishment of a mean gradient of velocity and turbulent eddies lead to transport. Care should be taken with this second definition, however, because "turbulent diffusion" is not true diffusion and can be reversed in a thermodynamic sense. Cases have been documented where cross-stream transport has led to rises in stagnation pressure along certain streamlines. Cross-transport of momentum is enhanced by the enlargement of eddies over the concave wall. These large eddies appear to exchange fluid across the edge of the boundary layer, the effect ranging as far out as two to three boundary layer thicknesses from the concave surface.

Cross-Stream Velocity Fluctuations

The streamwise evolution of profiles of the rms of radial velocity fluctuations, $\sqrt{\overline{v^2}}$, over the concave wall in the high-TI case is shown in Fig. 2. Distance from the wall is scaled on the boundary layer thickness. Evaluation of this thickness requires special processing, as discussed by Kestoras and Simon (1993). Over the concave wall, $\sqrt{\overline{v^2}}$ profiles exhibit a peak in the core of the flow ($y/\delta_{99.5} > 1$). As the edge of the boundary layer is approached by traversing from the core, $\sqrt{\overline{v^2}}$ values are damped. At $y/\delta_{99.5} \approx 0.2$ values of $\sqrt{\overline{v^2}}$ are only 75% of their peak value in the core of the flow. The damping of $\sqrt{\overline{v^2}}$ within the boundary layer over the concave wall in the high-turbulence case is in contrast to the behavior of $\sqrt{\overline{u^2}}$ values which rise above their core-flow values within the boundary layer (Kestoras and Simon, 1993). This damping is apparently more affected by the presence of the wall than is $\sqrt{\overline{u^2}}$. This was reported also by Thomas and Hancock (1977).

When TI is elevated, values of $\sqrt{\overline{v^2}}$ in the outer half of the boundary layer are increased (e.g. profile at station 5 in Fig. 3). Surprisingly, though, in the inner half of the boundary-layer ($y/\delta_{99.5} < 0.5$), values of $\sqrt{\overline{v^2}}$ in the presence of high-TI fall below values of $\sqrt{\overline{v^2}}$ taken in the low TI case (Fig. 3). It is possible that the

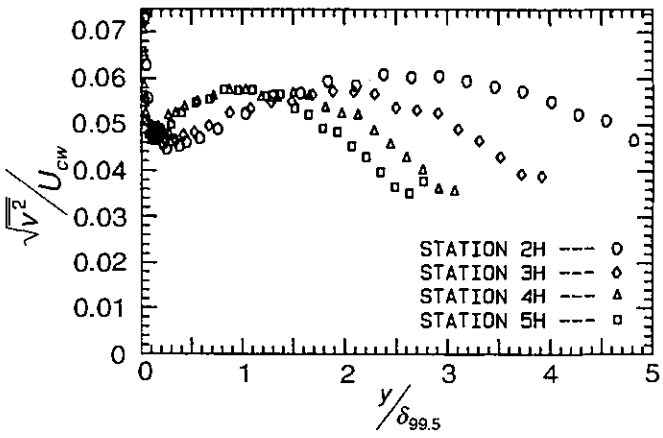

Fig. 2 Non-Dimensionalized Cross-stream Velocity Fluctuation over the Concave Wall, High-TI Case.

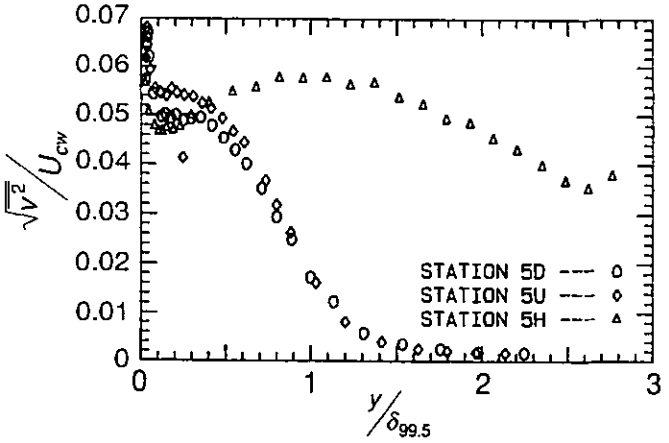

Fig. 3 Effect of Elevated TI on Cross-stream Velocity fluctuations over the Concave Wall. Station 5H, High-TI Case; Stations 5U and 5D, Upwash and Downwash of Low-TI case.

reduction in radial fluctuations in the high-turbulence case is a result of the absence of Görtler-like vortices. In the low-TI case, the effect of Görtler-like vortices penetrates deeply into the boundary layer over the concave wall causing values of $\sqrt{\overline{v^2}}$ at an upwash (U) site to be different than values at a downwash (D) site (stations 5U and 5D in Fig 3). Apparently, radial motions are particularly enhanced by the presence of Görtler-like vortices even very near the concave surface (Kestoras, 1993 and Barlow and Johnston, 1988). Elevation of free-stream turbulence intensity increases mean velocity as well as turbulence intensity in the near-wall region over the concave surface (Kestoras and Simon, 1993). Similarly, the effect of TI on $\sqrt{\overline{v^2}}$ values would be an increase. Therefore, the reduction in $\sqrt{\overline{v^2}}$ that is observed under high-TI conditions may be tied to the absence of Görtler-like vortices (Kestoras and Simon, 1993).

Another scenario is that Görtler-like vortices do form but they are not stationary. Instead, they meander around the concave surface, appearing and disappearing. If they were present, they must meander rapidly, for no stable pattern of their presence is visible on the liquid crystal sheet color pattern or in the thermocouple data. Görtler-like vortices did meander over the concave surface used by Barlow and Johnston (1988). The drop of $\sqrt{\overline{v^2}}$ values below those in the low-TI case may be giving a clue about the behavior of Görtler-like vortices in the high-TI case. Because of the action of Görtler-like vortices, values of $\sqrt{\overline{v^2}}$ at the upwash and downwash regions in the low-TI case are different from one another for

$y/\delta_{99.5}$ <0.5 (Fig. 3). A meandering of Görtler-like vortices in the high-turbulence case would have resulted in $\sqrt{\overline{v^2}}$ values that range from the upwash-site value observed in the low-TI case to the downwash-site value (assuming that the vortices are at least of the same strength as the vortices in the low-TI case), or, perhaps are somewhat higher in value than either, as a result of the unsteadiness of the meandering vortex. Figure 3, however, shows near-wall ($y/\delta_{99.5} < 0.25$) values of $\sqrt{\overline{v^2}}$ in the high-TI case that are lower than either the upwash- or the downwash-site values taken in the low-TI case. Thus, an absence of Görtler-like vortices in the high-turbulence case appears at his time to be more plausible than a scenario of meandering vortices.

Turbulent Shear Stresses

The streamwise evolution of shear stress values on the concave wall under high-TI conditions is shown in Fig. 4. Values of $-\overline{uv}$ within the boundary layer rise with streamwise distance over the initial part of the concave wall (stations 2H, 3H and 4H). On the latter portion (stations 4H and 5H), within measurement uncertainty, it appears that this streamwise evolution has stopped. The effect of free-stream turbulence on values of $-\overline{uv}$ over the concave wall is exemplified by profiles at station 4 of Fig. 5. Throughout the boundary layer, turbulent-shear-stress values on the concave wall in the high-TI case are above values obtained under very low-TI conditions. This may be explained by considering the production term of the $-\overline{uv}$ budget equation. The dominant terms are:

$$P_{-\overline{uv}} = (1 + y/R)\overline{v^2}\frac{\partial U}{\partial y} - \frac{U}{R}(2\overline{u^2} - \overline{v^2}) \qquad (2)$$

The near-wall mean strain (in general most of the production takes place near the wall), $\frac{\partial U}{\partial y}$, increases when TI is elevated (Kestoras and Simon, 1993). Thus, the first term of Eqn. 2 rises with the turbulence level ($\overline{v^2}$ does not decrease much in the region $y/\delta_{995}<0.1$ relative to the increase in $\frac{\partial U}{\partial y}$ in the same region). The second term also rises in the high-TI case because near the wall, $\overline{u^2}$ rises (Kestoras and Simon, 1993) while $\overline{v^2}$ drops (Fig. 3) relative to low-TI values. Since the radius of curvature, R, is negative for a concave surface, the contribution of both terms of Eqn. 2 increases in the near-wall region when free-stream turbulence is increased.

Turbulent shear stress values taken in the core of the flow over the concave wall may display the cross-transpon of momentum by boundary work discussed above. In the low-TI case (TI ~ 0.6%) very little cross transport of momentum takes place outside the boundary layer over the concave wall (Kestoras, 1993). Consequently, turbulent shear stress values diminish to zero outside the boundary layer. In contrast, when TI is increased, the core flow is unsteady and substantial cross-transport of momentum is taking place even outside the boundary layer over the concave wall. This is clearly indicated by the high Reynolds shear stress values throughout the core of the flow over the concave wall (Fig. 4, $y/\delta_{99.5}$)1).

Turbulent Heat Flux

The streamwise evolution of cross-stream turbulent heat-flux values in the high-turbulence case over the concave wall is shown in Fig. 6. Values of $\overline{vt}$ remain high outside the boundary layer ($y/\delta_{99.5}$)1). In fact, substantial cross-transport of heat is taking place as far as three boundary layer thicknesses from the concave wall. This is in contrast to the low-TI case, where turbulent heat flux values over the concave wall reduce to zero outside the boundary layer (Kestoras, 1993). The high values of $\overline{vt}$ outside the boundary layer may be the result of the enlargement of the eddies with

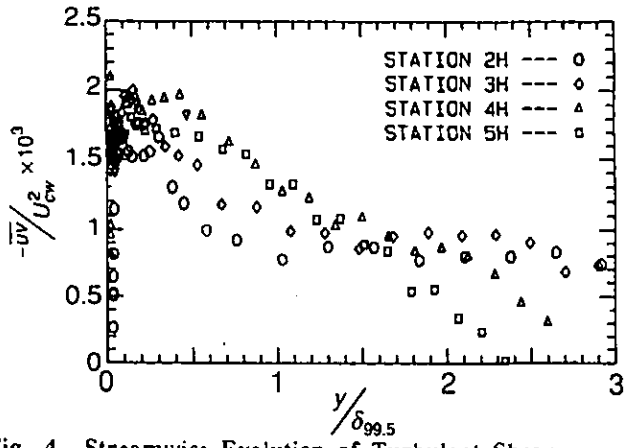

Fig. 4 Streamwise Evolution of Turbulent Shear Stresses over the Concave Wall, High-TI case.

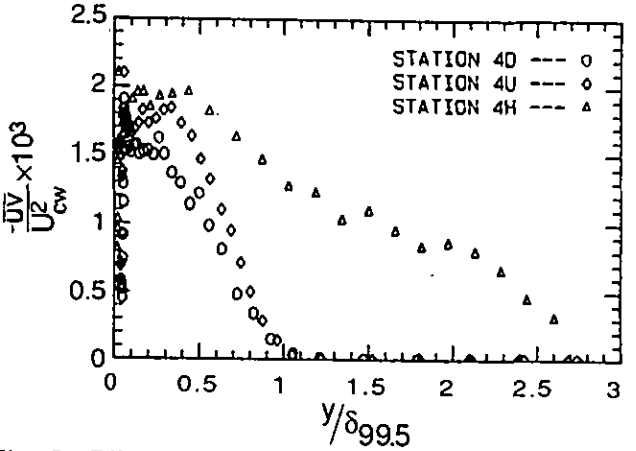

Fig. 5 Effect of Elevated TI on Profiles of Turbulent Shear Stresses over the Concave Wall. Stalion 4H -- High TI; Stations 4U and 4D, Upwash and Downwash of Low TI.

streamwise distance, as reported by Barlow and Johnson (1988). The large-scale eddies reach outside the boundary layer, intermittently boosting values of $\overline{vt}$ in the core of the flow. High values of $\overline{vt}$ are obtained well beyond the edge of the boundary layer throughout the entire concave section. This scenario is consistent with values of $\sqrt{\overline{t^2}}$ which remain high beyond the edge of the boundary layer (Fig. 9, to be presented). It is also consistent with the observations of Hancock and Bradshaw (1989); in a heated boundary layer, they reported that the intermittency in the wake region rises when free-stream turbulence is increased.

The effect of concave curvature on turbulent heat flux values within the boundary layer, in the high-TI case, is also shown in Fig. 6. Values of $\overline{vt}$ increase with streamwise distance. Turbulent shear stress values, $-\overline{uv}$, in the high-TI case exhibit similar behavior. It was indicated above, that the streamwise evolution of $-\overline{uv}$ (and $\overline{vt}$) may be tied to the enlargement of eddies with streamwise distance, as reported by Barlow and Johnston (1988).

The effect of free-stream turbulence on turbulent heat flux values over the concave wall is exemplified by the station 5 profiles in Fig. 7. High TI seems to increase values of $\overline{vt}$ mostly in the outer half of the boundary layer. However, very near the concave wall, $y/\delta_{99.5}$ (0.15 (Fig 7), the turbulent-heat-flux values in the presence of high TI are below the upwash and downwash site values of the low-TI case (see, for example, a minimum value of 0.72 at $y/\delta_{99.5}$ = 0.1). Low near-wall values over the concave wall are also observed in profiles of $\sqrt{\overline{v^2}}$ under high-TI conditions. The low values of $\overline{vt}$ (and

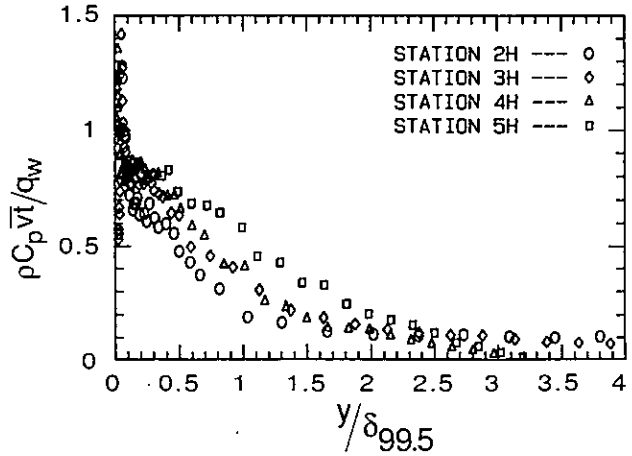

Fig. 6 Cross-Stream Turbulent Heat Fluxes over the Concave Wall. High-TI Case.

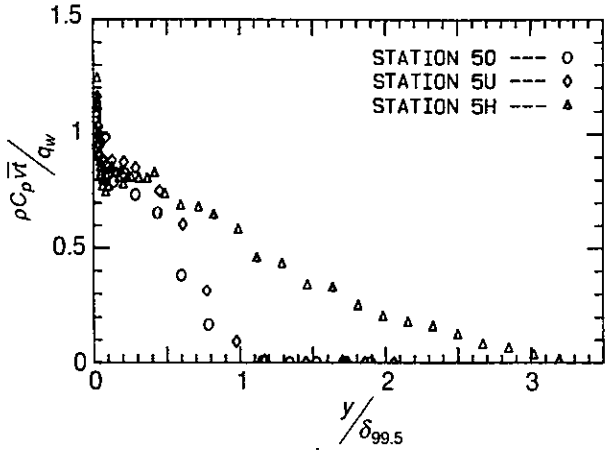

Fig. 7 Effect of TI on Cross-stream Turbulent Heat Fluxes over the Concave Wall. Station 5H -- High TI; Stations 5U and 5D, Upwash and Downwash of Low TI.

$\sqrt{\overline{v^2}}$), relative to those in the low-TI case, are believed to be the combined effects of two factors: (1) the inability of the large-scale, free-stream turbulence to penetrate and affect the near-wall region; and (2) the lack of enhancement of radial motions by Görtler-like vortices in the high-TI case. Görtler-like vortices are present and enhance radial motion and $\overline{vt}$ values in the low-TI case.

Streamwise Turbulent Heat Flux

Free-stream turbulence increases streamwise-turbulent-heat-flux values, $-\overline{ut}$, above low-TI values throughout the boundary layer on the concave wall (not shown). The increase becomes more profound with streamwise distance over the concave wall. The effects of free-stream turbulence on $-\overline{ut}$ values in the core of the flow over the concave wall are minimal, however.

Temperature Fluctuations

The effects of concave curvature on rms temperature fluctuations, $\sqrt{\overline{t^2}}$, in the high-TI case are shown in Fig. 8 (station 2H-5H). In the innermost 60% of the boundary layer, the rms variations of temperature fluctuations, $\sqrt{\overline{t^2}}$, decrease over the upstream one-third of the concave wall (stations 2H and 3H). Thereafter, profiles of $\sqrt{\overline{t^2}}$ in the innermost 60% of the boundary layer show little evolution (stations 4H and 5H). In contrast, in the outermost 40% of the boundary layer and in the core of the flow, values of $\sqrt{\overline{t^2}}$ rise with streamwise distance (stations 2H-5H). In the

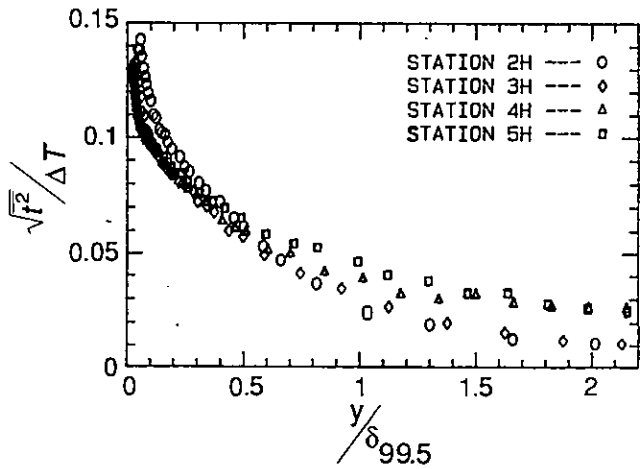

Fig. 8 Streamwise Evolution of Rms Temperature Fluctuations over the Concave Wall. High-TI Case.

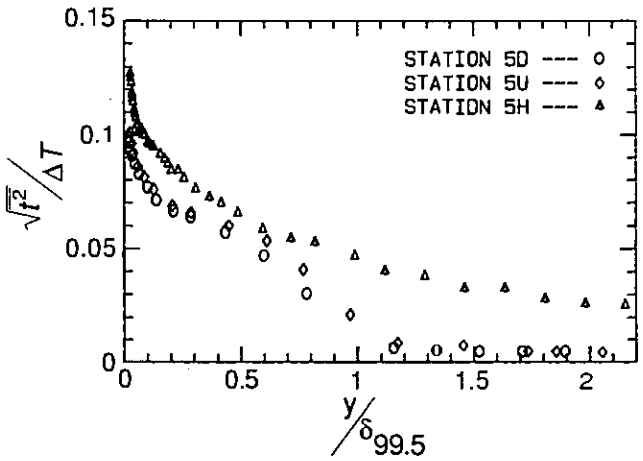

Fig. 9 Effect of TI on Rms Temperature Fluctuations on the Concave Wall. Station 5H -- High TI; Stations 5U and 5D, Upwash and Downwash of Low TI.

low-TI case, as a result of concave curvature, values of $\sqrt{\overline{t^2}}$ drop with streamwise distance throughout the boundary layer (Kestoras, 1993). Thus, in the outer part of the boundary layer, free-stream turbulence reverses this effect of concave curvature in these coordinates.

The effects of high-TI on $\sqrt{\overline{t^2}}$ values in the boundary layer over the concave wall is exemplified by the station 5 profiles in Fig. 9. High TI increases $\sqrt{\overline{t^2}}$ values (station 5H) throughout the boundary layer. Even near the wall, the rise in $\sqrt{\overline{t^2}}$ values is remarkable; at $y/\delta_{99.5} \approx 0.1$, $\sqrt{\overline{t^2}}$ values (station 5H) increase by almost 20%. This rise is in contrast to the behavior of $\sqrt{\overline{v^2}}$, $\overline{vt}$, and $-\overline{ut}$ (Figs. 3 and 7) which do not rise in the near-wall region when TI is elevated. Possible explanations are currently being sought. Clearly, a different boundary condition on $\sqrt{\overline{t^2}}$ exists compared to $\sqrt{\overline{v^2}}$. The velocity fluctuation must be zero at the wall, whereas the wall skin temperature is allowed to fluctuate.

Eddy Diffusivity of Momentum

Turbulence activity over the concave wall, as measured by the eddy diffusivity of momentum, ε_m, increases with streamwise distance over the concave wall in the high-TI case (Fig 10). The rise

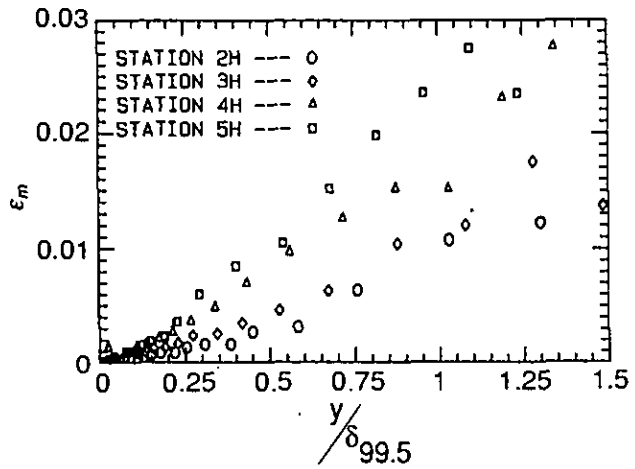

Fig. 10 Streamwise Evolution of Eddy Diffusivity of Momentum over the Concave Wall. High-TI Case.

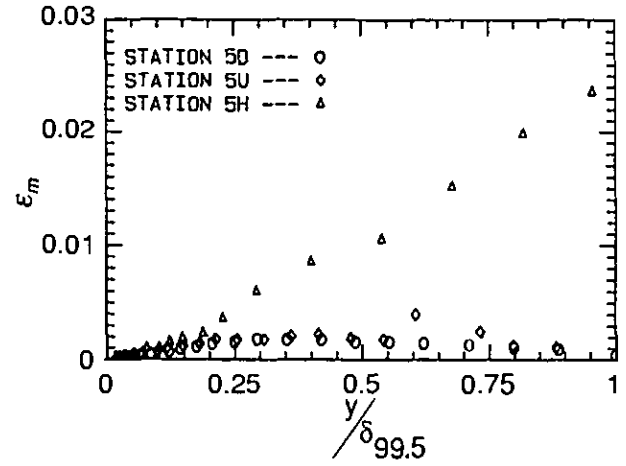

Fig. 11 Effect of TI on Eddy Diffusivity of Momentum on the Concave Wall. Station 5H -- High TI; Stations 5U and 5D -- Upwash and Downwash of Low TI Case.

in values of ε_m diminishes on the latter parts of the concave wall (stations 4H and 5H). Again, the rapid increase in values of ε_m upstream on the concave wall may be tied to the enlargement of large-scale eddies and their migration towards the concave surface (Barlow and Johnston, 1988). The effect of high free-stream turbulence intensity is exemplified by station 5 profiles in Fig. 11. At $y/\delta_{99.5} \approx 0.5$, values of ε_m in the high-turbulence case are nearly eight-times the values of ε_m in the low-turbulence case (stations 5D and 5U). Under low-TI conditions, profiles of ε_m over the concave wall exhibit a peak whereas at elevated TI, profiles of ε_m do not. Instead, they rise almost linearly with normal distance from the wall throughout the boundary layer. It may be that this rise, even outside the boundary layer, is effected by the enlargement of the eddies and cross transport of momentum by boundary work, as discussed in the analysis of turbulent shear stresses.

Profiles of the eddy diffusivity of heat, ε_h, (not shown) exhibit a similar behavior.

Mixing Length of Momentum

The effect of concave curvature on values of mixing length, in the high-turbulence case is shown in Fig. 12. In the inner part of

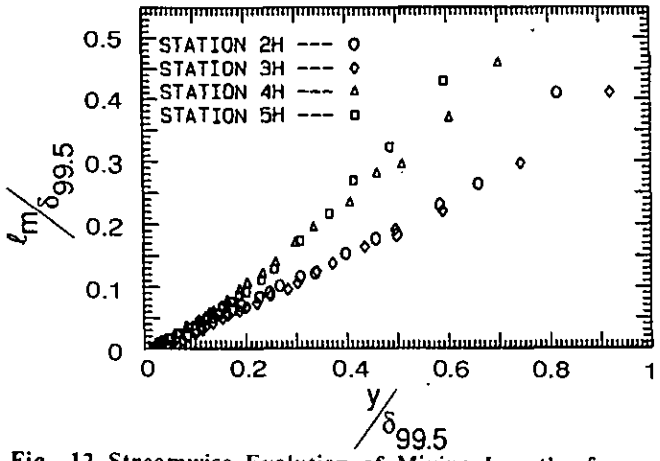

Fig. 12 Streamwise Evolution of Mixing Length of Momentum over the Concave Wall. High-TI Case.

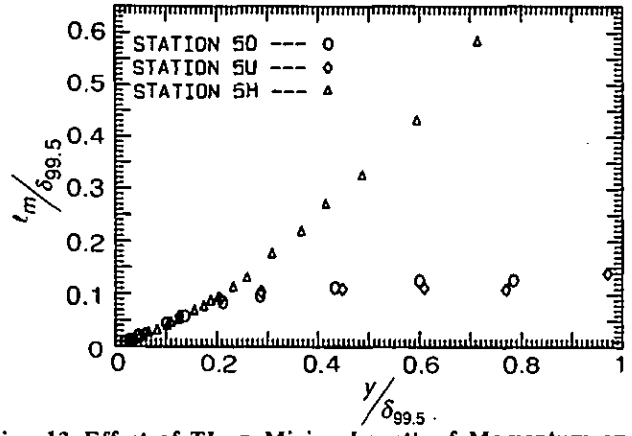

Fig. 13 Effect of TI on Mixing Length of Momentum on the Concave Wall. Station 5H -- High TI; Stations 5U and 5D -- Upwash and Downwash of Low TI Case.

the boundary layer, $y/\delta_{99.5} < 0.2$, values of ℓ_m increase only slightly with streamwise distance on the concave wall (station 2H-5H). The slope of these profiles in the region $y/\delta_{99.5} < 0.2$ is 0.41, the value exhibited on a flat wall, known as the Kármán constant. Inner-layer profiles of ℓ_m in the low-TI case also show this slope. Early upstream on the concave wall, under high-TI conditions (station 2H and 3H in Fig. 12), mixing length profiles show no evolution throughout the entire boundary layer. In fact, the near-wall slope at these stations, appears to hold out to $y/\delta_{99.5} = 0.7$. On the latter parts of the concave wall (station 4H), however, mixing length profiles in the region $y/\delta_{99.5} > 0.2$ become abruptly steeper than upstream profiles. Thereafter, the mixing length profiles in the region $y/\delta_{99.5} > 0.2$ continue steepening with streamwise distance over the concave wall. However, the rate of increase in slope diminishes (stations 4H and 5H). The increasing values of ℓ_m with streamwise distance may be a manifestation of the larger-scale eddies growing and approaching the concave wall, as reported by Barlow and Johnston (1988). The effect of high TI on values of mixing length, ℓ_m, over the concave wall is depicted in the station 5 profiles of Fig. 13. Mixing length values in the high-TI case (station 5H) grow almost linearly with y-distance throughout the boundary layer over the concave wall (station 5H). In the low-TI case, mixing length values (stations 5D and 5U) become level in the outer part of the boundary layer over the concave wall.

Mixing length distributions in the high-TI case, over the concave wall (station 5H in Fig. 13), when compared with distributions in the low-TI case (stations 5U and 5D in Fig. 13), show the importance of the innermost 20% of the boundary layer in determining wall mean values (e.g. C_f, St, etc.); in 80% of the boundary layer over the concave wall, ℓ_m values in the high-turbulence case (station 5H) are much higher than values at the downwash regions in the low-TI case (station 5D). Yet, skin friction coefficients in the high-TI case are only slightly higher than values in the downwash region over the concave wall.

Profiles of mixing length of heat, under high-TI conditions exhibit a behavior similar to that exhibited by mixing length of momentum.

Turbulent Prandtl Number

The streamwise evolution of turbulent Prandtl numbers, P_{rt}, in the high-TI case on the concave wall is shown in Fig. 14. The single-sample uncertainty in Pr_t values is 0.2 - 0.25 in the inner half of the boundary layer. The large scatter is consistent with this uncertainty value. General levels based upon several values can be stated with lower uncertainty, about 10% for a pooled sample of four. Some indications of the effect of concave curvature on Pr_t can be discerned in spite of the high uncertainty in these measurements. Values of P_{rt} in the high-TI case seem to rise with streamwise distance over the upstream part of the concave wall (station 2H-4H) then drop rather precipitously at station 5H. Average values rise from 0.9 to 1.3, then drop again to 0.9. This behavior of Pr_t values ($P_{rt} = \varepsilon_m/\varepsilon_h$) reveals that for most of the concave wall, the turbulent transport of momentum is rising faster with streamwise distance than is the turbulent transport of heat. The improved turbulent transport of momentum within the flow is consistent with the behavior at the wall; upstream skin friction coefficients in the high-TI case rise faster than Stanton numbers (Kestoras and Simon, 1993). Stanton numbers do rise appreciably on the latter parts of the concave wall. This rise in Stanton number implies an improved turbulent transport of heat which is consistent with the drop in turbulent Prandtl numbers at the last station (station 5H) on the concave wall.

The effects of TI on Pr_t values on the concave wall are also somewhat obscured by the scatter of the data (see Fig. 15, where only profiles at station 4 are shown). It appears that a Pr_t value around 1.1 would suffice in modeling a heated turbulent boundary layer over a concave wall under low-TI conditions whereas a 20% larger value may be more appropriate for elevated TI conditions.

Cross-Stream Transport of Turbulent Shear Stress

The streamwise evolution of cross transport of shear stress values, $\overline{uv^2}$, on the concave wall in the high-TI case is shown in Fig. 16. Values of $\overline{uv^2}$ gradually but monotonically rise with streamwise distance on the concave wall (stations 2H-5H). By the end of the concave wall (stations 4H and 5H) values of $\overline{uv^2}$ generally show a reduced rate of evolution (particularly, within the inner half of the boundary layer). The cross transport of shear stress, $\overline{uv^2}$, is primarily the result of large-scale eddy motions. Thus, the rise in $\overline{uv^2}$ values with streamwise distance, may be a manifestation of a growth of large-scale eddies, as discussed above. Profiles of mixing length of momentum, ℓ_m, indicate that the enlargement caused by the concave curvature in the high-TI case is more profound than in the case of low TI (Fig. 13). It therefore appears that the effect of concave curvature on $\overline{uv^2}$ is enhanced by the presence of particularly large-scale eddies outside the boundary layer. It is remarkable that values of $\overline{uv^2}$ rise even in the core of the flow over the concave wall $y/\delta_{99.5} > 1$ when TI is elevated. Such a rise implies that the effect of curvature on $\overline{uv^2}$ propagates to the region outside the boundary layer. Apparently, augmentation by concave curvature more than compensates for the decay of turbulence.

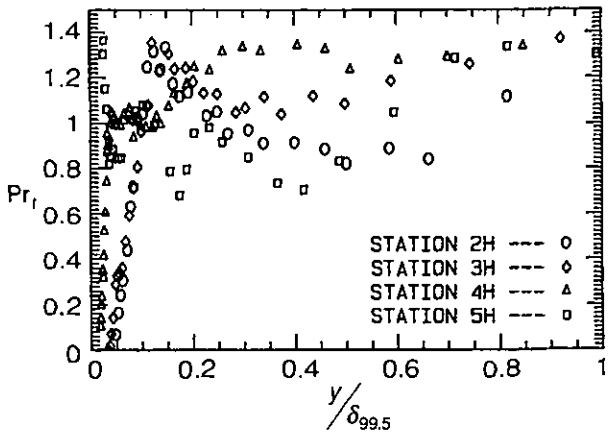

Fig. 14 Streamwise Evolution of Turbulent Prandtl Number over the Concave Wall. High-TI Case.

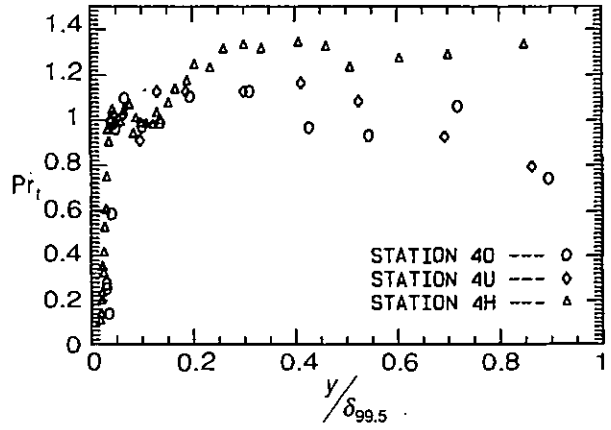

Fig. 15 Effect of TI on Turbulent Prandtl Number on the Concave Wall. Station 4H -- High TI; Stations 4U and 4D, Upwash and Downwash of Low TI Case.

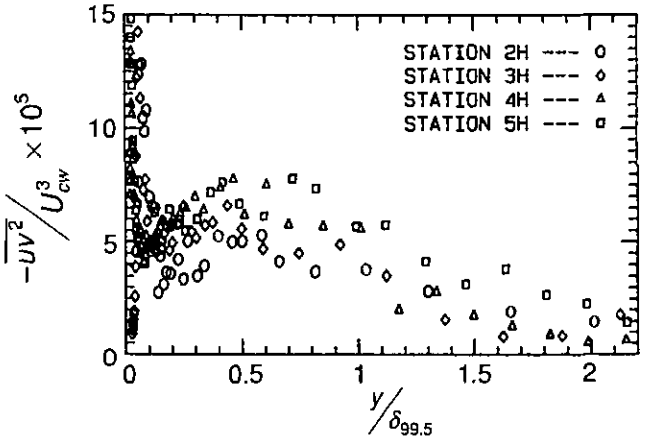

Fig. 16 Streamwise Evolution of Cross-Stream Transport of Turbulent Shear Stresses over the Concave Wall. High-TI Case.

The effect of free-stream turbulence on values of $\overline{uv^2}$ on the concave wall in the high-TI case is shown in Fig. 17 (for station 4). Profiles of $\overline{uv^2}$, with low- and high-TI have similar shapes. However, values in the high-turbulence case are higher; the peak value of $\overline{uv^2}$ doubles when TI is elevated.

Profiles of cross-stream transport of turbulent heat flux, $\overline{v^2t}$ (not shown) show similar behavior.

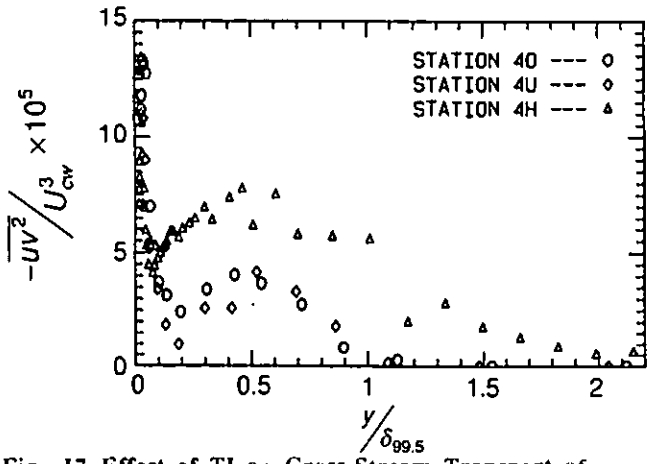

Fig. 17 Effect of TI on Cross-Stream Transport of Turbulent Shear Stresses on the Concave Wall. Station 4H -- High TI; Stations 4U and 4D, Upwash and Downwash of Low TI.

Conclusions

1) Cross transport of streamwise momentum is reported outside the boundary layer over the concave wall when TI is elevated. The cross transport is a result of boundary work performed by unsteady streamtubes in the presence of a cross-stream pressure gradient.

2) High TI enhances turbulent quantities, $\sqrt{\overline{v^2}}$, $\overline{vt}$, $\overline{-uv}$ etc. in the outer region of the boundary layer over the concave wall.

3) Values of $\sqrt{\overline{v^2}}$ and $\overline{vt}$ are reduced near the concave surface when the free-stream turbulence is enhanced. This is believed to be a result of the absence of Görtler-like vortices whose presence in the low-TI case enhances radial motions. Values of $\sqrt{\overline{v^2}}$ and $\overline{vt}$ near the wall in the high-TI case are lower than either the upwash of downwash values of the low-TI case. This tends to refute the scenario of meandering Görtler-like vortices.

4) Large scale eddies cause high $\overline{vt}$ and $\sqrt{\overline{t^2}}$ values in the core of the flow over the concave wall. These eddies enlarge with streamwise distance.

5) In the high-TI case, mixing length profiles over the concave wall in the region $y/\delta_{99.5} < 0.2$ have the same slope as profiles in the low-TI case, described by the Kármán constant. For $y/\delta_{99.5} > 0.2$ mixing lengths grow almost linearly with the normal distance from the wall, whereas they level off in the low-TI case.

6) Turbulent Prandtl numbers, in the high-TI case, rise with streamwise distance over the concave wall from the value of 0.9 to 1.3. At the latter part of the concave wall they drop back to 0.9.

Acknowledgments

Support for this work from the Air Force Office of Scientific Research (grant number AF/AFOSR-91-0322) is gratefully acknowledged. The project monitor is Major Daniel Fant.

References

Barlow, S.R., and Johnston, J.P., (1988), "Structure of a Turbulent Boundary Layer on a Concave Surface," J. Fluid Mech., Vol. 191, pp. 137-176.

Blair, M. F., (1983), "Influence of Free-Stream Turbulence on Turbulent Boundary Layer Heat Transfer and Mean Profile Development, Part II-Analysis of Results", J. of Heat Transfer, Vol. 105, pp.41-47.

Brown, A., and Burton, R. C., (1977), "The Effects of Free-Stream Turbulence Intensity and Velocity Distribution on Heat Transfer to Curved Surfaces", ASME Paper 77-GT-48.

Champagne, F.H., Sleicher, C.A., and Wehrmann, O.H., (1967), "Turbulence Measurements with Inclined Hot-Wires, Parts 1 and 2," J. Fluid Mech., Vol. 28, pp. 153-182.

Eckert E. R. G., (1987) "Cross Transport of Energy in Fluid Streams," Wärme-und Stoffübertragung, Vol. 21, pp. 73-81.

Görtler, H., 1940, "Über ein Dreidimensionale Instabilitat Laminarer Grenzschichten an Konkaven Wanden," Math.-Phys., K1.2:1; also NACA TM-1375, 1954.

Hancock, P. E., and Bradshaw, P., (1983), "The Effect of Free-Stream Turbulence on Turbulent Boundary Layers", Transactions of the ASME, Vol. 105, pp. 284-289.

Hancock, P. E., and Bradshaw, P., (1989), "Turbulence Structure of a Boundary Layer Beneath a Turbulent Free-Stream", J. Fluid Mech., Vol. 205, pp. 45-76.

Hishida, H., and Nagano, Y., (1978), "Simultaneous Measurements of Velocity and Temperature in Nonisothermal Flows," J. of Heat Transfer, Vol. 100, No. 2, pp. 340-345.

Hoffmann, P.H., Muck, K.C.B., and Bradshaw, P., (1985), "The Effect of Concave Curvature on Turbulent Boundary Layers," J. Fluid Mech, Vol. 161, pp. 371-403.

Hunt, J.C.R. and Graham, J.M.R., (1978), "Free-stream turbulence near plane boundaries," J. Fluid Mech., Vol. 84, pp. 209-235.

Kestoras, M.D., and Simon, T.W., (1992), "Hydrodynamic and Thermal Measurements in a Turbulent Boundary Layer Recovering from Concave Curvature," ASME J. of Turbomachinery, Vol. 114, No. 4, pp. 891-898.

Kestoras, M. D., (1993), Heat Transfer and Fluid Mechanics Measurements in a Turbulent Boundary Layer: Introduction and Removal of Concave Curvature under High Free-Stream Turbulence Conditions, Ph.D. Thesis, Dept. of Mech. Engrg., University of Minnesota.

Kestoras, M. D., Simon, T. W., (1993), "Combined Effects of Concave Curvature and High Free-Stream Turbulence Intensity on Boundary Layer Heat and Momentum Transport", ASME Paper 93-WA/HT-56.

Kim, J., (1986), "The Development of a Turbulent Heat Flux Probe and its Use in a 2-D Boundary Layer over a Convex Surface," MSME Thesis, Dept. of Mech. Engrg., University of Minnesota.

Kim, J., and Simon, T.W., (1988), "Measurements of the Turbulent Transport of Heat and Momentum in Convexly Curved Boundary Layers: Effects of Curvature, Recovery and Free-Stream Turbulence," J. of Turbomachinery, Vol. 110, No. 1, pp. 80-87.

Kim, J., Simon, T.W., and Russ, S.G., (1992), "Free-stream Turbulence and Concave Curvature Effects on Heated, Transitional Boundary Layers," J. of Heat Transfer, Vol. 114, No. 2, pp. 339-347.

Nakano, S., Takahashi, A., Shizawa, T. and, Honami, S., (1981), "Effects of Stable and Unstable Free-Streams on a Turbulent Flow Over a Concave Surface", Proc. 3rd Symposium on Turbulent Shear Flows, Davis, CA.

O'Brien, J.E. and vanFossen, G.J. (1985) "The Influence of Jet Grid Turbulence on Heat Transfer from the Stagnation region of a Cylinder in Cross Flow", ASME 85-HT-58.

Ramaprian, B.R., and Shivaprasad, B.G., (1977), "Mean Flow Measurements in Turbulent Boundary Layers along Mildly Curved Surfaces," AIAA J., Vol. 15, No. 2, pp. 189-196.

Ramaprian, B.R., and Shivaprasad, B.G., (1978), "The Structure of Turbulent Boundary Layers along Mildly Curved Surfaces", J. Fluid Mechanics., Vol. 85, part 2, pp. 273-303.

Shizawa, T., and Honami, S., (1985), "Experiments on a Turbulent Boundary Layers over a Concave Surface - Response of Turbulence to Curvature", 5th Symposium on Turbulent Shear Flows, Ithaca, August 1985.

So, R.M. and Mellor, G.L., (1975), "Experiment on Turbulent Boundary Layers on a Concave Wall." The Aeronautical Quarterly, Vol. 26, pp. 25-40.

Tani, I., 1962, "Production of Longitudinal Vortices in the Boundary Layer Along a Concave Wall", J. of Geophysical Research, Vol. 67, p. 3075.

Thomas, N.H. and Hancock P.E., (1977), "Grid Turbulence Near a Moving Wall", J. Fluid Mech., Vol. 82, pp. 481-496.

Wang, T., (1984), "An Experimental Investigation of Curvature and Freestream Turbulence Effects on Heat Transfer and Fluid Mechanics in Transition Boundary Layer Flows," Ph.D. Thesis, University of Minnesota.

Yavuzkurt, S., (1984), "A guide to Uncertainty Analysis of Hot-Wire Data," J. Fluids Engineering, Vol. 106, pp. 181-186.

You, S.M., Simon, T.W., and Kim, J., (1986), "Boundary Layer Heat Transfer and Fluid Mechanics Measurements on a Mildly-curved Convex Wall," Proc. 8th Int. Heat Transfer Conf., Vol. 3, pp. 1089-1094.